THE JOURNAL OF BIOLOGICAL CHEMISTRY
Vol. 276, No. 19, Issue of May 11, pp. 16076–16082, 2001

Printed in U.S.A.

The Structure of the Multidrug Resistance Protein 1 (MRP1/ABCC1)

CRYSTALLIZATION AND SINGLE-PARTICLE ANALYSIS*

Received for publication, January 9, 2001
Published, JBC Papers in Press, January 22, 2001, DOI 10.1074/jbc.M100176200

Mark F. Rosenberg‡§, Qingcheng Mao¶, Andreas Holzenburg‖, Robert C. Ford‡, Roger G. Deeley¶, and Susan P. C. Cole¶

From the ‡Department of Biomolecular Sciences, University of Manchester Institute of Science and Technology, Manchester M60 1QD, United Kingdom, ¶Cancer Research Laboratories, Queen's University, Kingston, Ontario K7L 3N6, Canada, and the ‖Electron Microscopy Center and Department of Biology, Texas A&M University, College Station, Texas 77843-2257

Multidrug resistance protein 1 (MRP1/ABCC1) is an ATP-binding cassette (ABC) polytopic membrane transporter of considerable clinical importance that confers multidrug resistance on tumor cells by reducing drug accumulation by active efflux. MRP1 is also an efficient transporter of conjugated organic anions. Like other ABC proteins, including the drug resistance conferring 170-kDa P-glycoprotein (ABCB1), the 190-kDa MRP1 has a core structure consisting of two membrane-spanning domains (MSDs), each followed by a nucleotide binding domain (NBD). However, unlike P-glycoprotein and most other ABC superfamily members, MRP1 contains a third MSD with five predicted transmembrane segments with an extracytosolic NH_2 terminus. Moreover, the two nucleotide-binding domains of MRP1 are considerably more divergent than those of P-glycoprotein. In the present study, the first structural details of MRP1 purified from drug-resistant lung cancer cells have been obtained by electron microscopy of negatively stained single particles and two-dimensional crystals formed after reconstitution of purified protein with lipids. The crystals display *p*2 symmetry with a single dimer of MRP1 in the unit cell. The overall dimensions of the MRP1 monomer are ~80 × 100 Å. The MRP1 monomer shows some pseudo-2-fold symmetry in projection, and in some orientations of the detergent-solubilized particles, displays a stain filled depression (putative pore) appearing toward the center of the molecule, presumably to enable transport of substrates. These data represent the first structural information of this transporter to ~22-Å resolution and provide direct structural evidence for a dimeric association of the transporter in a reconstituted lipid bilayer.

The 190-kDa multidrug resistance protein MRP1[1] (ABCC1) is a polytopic membrane transport protein that belongs to the ATP-binding cassette (ABC) superfamily and has been detected in many different drug-resistant cell lines and tumor tissues since it was first cloned in 1992 (1–6). When overexpressed in tumor cells, MRP1 confers multidrug resistance by reducing intracellular drug concentrations in an ATP-dependent manner (6–8). In this respect, MRP1 is similar to another ABC transporter, the well characterized 170-kDa P-glycoprotein (P-gp) (ABCB1) (9, 10). ABC proteins play important physiological and protective functions in bacteria, yeast, plants, and mammals and are capable of transporting a wide variety of molecules across biological membranes. Known substrates for ABC transporters include ions, phospholipids, steroids, polysaccharides, amino acids, peptides, and in the case of several MRP-related proteins, anionic conjugated endo- and xenobiotics (6, 10–12). In addition to MRP1 and P-gp, other examples of clinically important human ABC proteins include the cystic fibrosis transmembrane conductance regulator CFTR (13), and the sulfonylurea receptor (SUR), which is part of an ATP-sensitive potassium channel involved in insulin secretion (14).

The amino acid sequence of MRP1 predicts that it contains a core structure that is common to many ABC proteins, namely two hydrophobic membrane-spanning domains (MSDs) each followed by a nucleotide binding domain (NBD) (1). Most current evidence suggests that these two MSDs each consist of six transmembrane α-helices (15–18) and that the two NBDs are located on the cytoplasmic face of the plasma membrane (6, 19). In addition to this core, four-domain structure is a third, NH_2-proximal MSD (MSD1) of ~200 amino acids with an extracytosolic NH_2 terminus that is thus far found only in MRP1, SUR, and several other members of ABC subfamily "C" (1, 6, 12, 17). Certain modifications of MSD1 and the intracellular loop connecting it to MSD2 can inactivate the protein (20, 21), suggesting that interaction of MSD1 with other domains may play an important role in the regulation of MRP1 activity.

Transport studies using both MRP1-enriched plasma membrane vesicles and purified reconstituted MRP1 have established that MRP1 can actively transport a structurally diverse array of conjugated organic anions, including the cysteinyl leukotriene LTC_4 and oxidized glutathione (6, 12, 22–24). In contrast, studies using MRP1-enriched plasma membrane vesicles under similar conditions have failed to demonstrate that MRP1 directly transports unmodified chemotherapeutic agents (12, 26, 27). However, recent studies suggest that certain unconjugated drugs such as vincristine and daunorubicin are actively co-transported by MRP1 with reduced glutathione (25–27). These transport properties of MRP1 are quite different from those described for P-gp, and the structural features responsible for these differences between the two drug resistance proteins are not yet known. Indeed, little is known about the structure of MRP1.

* Supported in part by the Medical Research Council of Canada (Grant MT-10519). The costs of publication of this article were defrayed in part by the payment of page charges. This article must therefore be hereby marked "*advertisement*" in accordance with 18 U.S.C. Section 1734 solely to indicate this fact.

§ Recipient of a fellowship from the Royal Society (London, UK). To whom correspondence should be addressed: Tel.: 44-161-200-4186; Fax: 44-161-236-0409; E-mail: mark.rosenberg@umist.ac.uk.

[1] The abbreviations used are: MRP1, multidrug resistance protein 1; P-gp, P-glycoprotein; ABC, ATP-binding cassette; MSD, membrane-spanning domain; NBD, nucleotide-binding domain; LTC_4, leukotriene C_4; CHAPS, 3-[(3-cholamidopropyl)dimethylammonio]-1-propanesulfonic acid; CFTR, cystic fibrosis transmembrane regulator; SUR, sulfonylurea receptor; DDM, *n*-dodecyl-β-D-maltoside; IQ, signal-to-noise ratio.

We recently reported immunoaffinity purification of native MRP1 from the highly drug-resistant lung cancer cell line, H69AR, from which MRP1 was originally cloned (1, 24, 28). The purified reconstituted native protein exhibits low level basal ATPase activity that is stimulated by its organic anion substrates (28). More recently, we have demonstrated ATP-dependent transport of LTC_4 and other substrates in an artificial lipid bilayer system containing purified MRP1 (24). These data support the concept that MRP1 functions as an energy-dependent efflux pump, which couples translocation of its substrates with ATP hydrolysis. To understand the molecular mechanisms by which MRP1 recognizes and transports its substrates, and how this is coupled to ATP hydrolysis, it is desirable to obtain high resolution structural information on the protein. We have previously reported the low resolution structure of P-gp (29, 30), as determined by electron microscopy of single particles (31) and small epitaxial two-dimensional crystals and more recently, from larger two-dimensional crystals[2] by electron crystallography (32). In the present paper, we have obtained structural data for MRP1 up to ~22-Å resolution using similar approaches and describe the first two-dimensional crystals of this transporter in the presence of phospholipids. Analysis of the two-dimensional crystals in negative stain suggests that MRP1 acts as a dimer. This structural information provides a basis for further mechanistic studies of MRP1 and related ABC proteins.

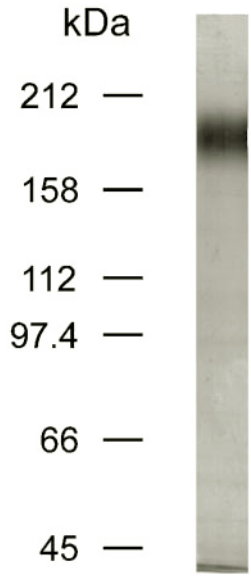

FIG. 1. **Polyacrylamide gel electrophoresis of solubilized immunoaffinity-purified native MRP1.** One microgram of purified native MRP1 was subjected to electrophoresis on a 7.5% w/v polyacrylamide gel and detected by alkaline silver staining. Molecular mass markers (kDa) are on the *left*.

EXPERIMENTAL PROCEDURES

Materials—Copper electron microscope grids and uranyl acetate were purchased from Agar Scientific (Essex, UK). Dimyristoyl L-α-phosphatidylcholine was from Sigma (Gillingham, Dorset, UK) and *n*-dodecyl-β-D-maltoside (DDM) was from Calbiochem (Nottingham, UK). Bio-Beads were obtained from Bio-Rad (Hertfordshire, UK). 3-[(3-Cholamidopropyl)dimethylammonio]-1-propanesulfonic acid (CHAPS) was from ICN (Aurora, OH).

Purification of MRP1—Plasma membranes were prepared as described previously from the doxorubicin-selected multidrug-resistant small cell lung cancer cell line H69AR (25). Plasma membranes containing MRP1 were solubilized with CHAPS and subjected to immunoaffinity chromatography as described in a previous study (24). Purity was estimated by densitometric scanning of polyacrylamide gels stained with alkaline silver and by immunoblotting (24) and only preparations of ≥90% purity were used for subsequent electron microscopy. In addition, all preparations of purified MRP1 used were reconstituted into proteoliposomes and tested for ATPase activity and transport activity as described previously (24, 28).

Single-particle Analysis of Negatively Stained MRP1—Purified MRP1 (12 μg ml^{-1}) was applied to freshly glow-discharged 400-mesh copper/carbon grids for 30 s and negatively stained in 4% w/v uranyl acetate (1 min). Scattered electrons from the stain dominate the images from negative staining, and thus, the protein is seen in negative. However, negative stain can readily provide information on the size, shape, and oligomeric form of MRP1. Electron micrographs were recorded at calibrated magnifications in a Philips CM 100 and a Tecnai 10-transmission electron microscope operating at 100 kV under low dose conditions. Images were recorded on Agfa Scientia film and developed for 4 min in PQ developer. The quality of the micrographs was checked on an optical diffractometer for astigmatism and drift, and suitable films were digitized at 4.2 Å per pixel at the specimen level using a Zeiss SCAI microdensitometer. Six hundred well- separated particles were interactively selected using Ximdisp, which comprises part of the MRC image-processing suite (33). Images were processed using the SPIDER image-processing software (31, 34) with reference-free alignment (35). Images were initially low-pass-filtered (filtering low resolution information) using a Gaussian band-pass filter to ~27-Å resolution, and the shifts and rotations were applied to the unfiltered images. The alignment converged after six rounds producing only a small change in the alignment parameters. The images were subjected to correspondence analysis and classification (36) with each class representing a relatively homogeneous subgroup of images. Each class was aligned separately, and average images were calculated by summing the aligned particles within one appropriate class (29). Symmetry was tested by a rotational autocorrelation search.

Two-dimensional Crystals of MRP1 and Image Processing—Purified MRP1 (~100 μg ml^{-1}) was reconstituted with dimyristoyl L-α-phosphatidylcholine at a protein/lipid ratio of 0.5–1.0 (w/w) with lipids solubilized in 0.1% (w/v) DDM in 50 mM Tris-HCl (pH 7.5) buffer containing 3 mM NaN_3. The detergent was removed over 6 h using SM2-Bio-Beads (15 g 100 ml^{-1}) at 22 °C. Electron microscope grids were prepared as above by negative staining by allowing 5 μl of the reconstituted vesicles to sit for 1 min on a 400-mesh glow-discharged carbon-coated copper grid. Excess solution was removed, and the specimen was negatively stained with 4% (w/v) uranyl acetate (1 min) and blotted. Patches of two-dimensional crystals (unit cell ~ 139 × 256 Å) were observed in some vesicles after 6-h incubation with Bio-Beads. Controls with protein omitted showed no crystals. Images were recorded and scanned as described above. Images were screened using an optical diffractometer for drift and astigmatism and to check for crystalline arrays of MRP1. Processing of images by correcting for the distortions in the crystal lattice (lattice unbending) and effects of the contrast transfer function and astigmatism was performed using the MRC-LMB software (33). Comparison of phase residuals (37) suggested *p*2 symmetry and is discussed below. Projection maps of the merged data were calculated using the standard crystallographic computer programs in the CCP4 package (38).

RESULTS

Purification of MRP1—MRP1 purity was judged to be greater than 90% based on the following criteria: (i) detection of a single band in an alkaline silver-stained gel of the protein resolved by polyacrylamide gel electrophoresis (Fig. 1), (ii) its homogeneity, as assessed by electron microscopy (Fig. 2), and (iii) its ability to crystallize (Fig. 5). ATPase and transport assays of the reconstituted purified protein confirmed that it was active and its activity could be inhibited by conformation-dependent MRP1-specific monoclonal antibodies (24, 28, 39). To obtain initial structural data for detergent-solubilized MRP1, samples were analyzed by electron microscopy of single particles.

Single-particle Analysis of MRP1—Fig. 2 shows a transmission electron micrograph of a negatively stained preparation of purified MRP1 in DDM (*panel a*) and a montage of representative MRP1 molecules (*panel b*) (the protein appears as *light shades* and stain as *dark shades*). The visualized particles were

[2] M. F. Rosenberg, G. Velarde, R. C. Ford, C. Martin, G. Berridge, I. D. Kerr, R. Callaghan, A. Schmidlin, C. Wooding, K. J. Linton, and C. F. Higgins, manuscript submitted.

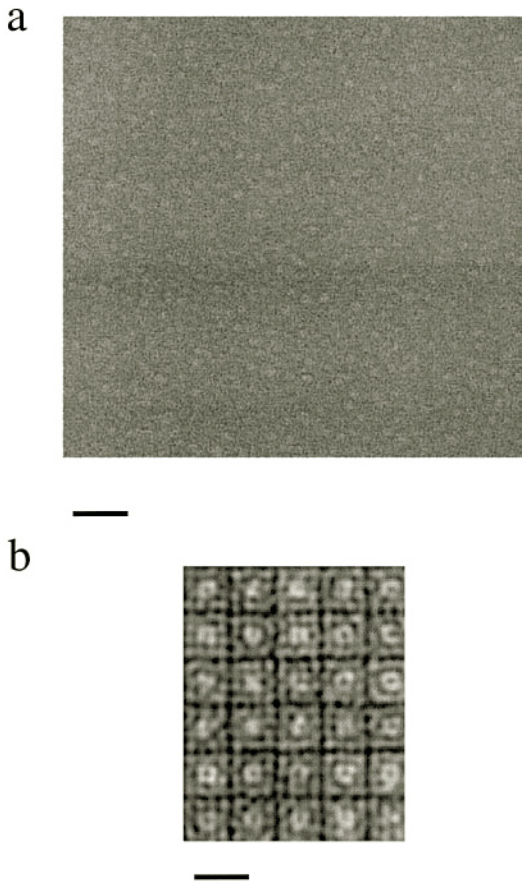

FIG. 2. **Electron microscopy of CHAPS-solubilized MRP1 in uranyl acetate.** *a*, the majority of the particles were ~100 Å in diameter. *b*, galleries of typical low-pass-filtered molecules, to ~35-Å resolution, shown at higher magnification, which were selected for single-particle analysis. A stain-filled cavity is evident in some of the molecules. The *scale bar* in *a* shows 500 Å and in *b* shows 250 Å.

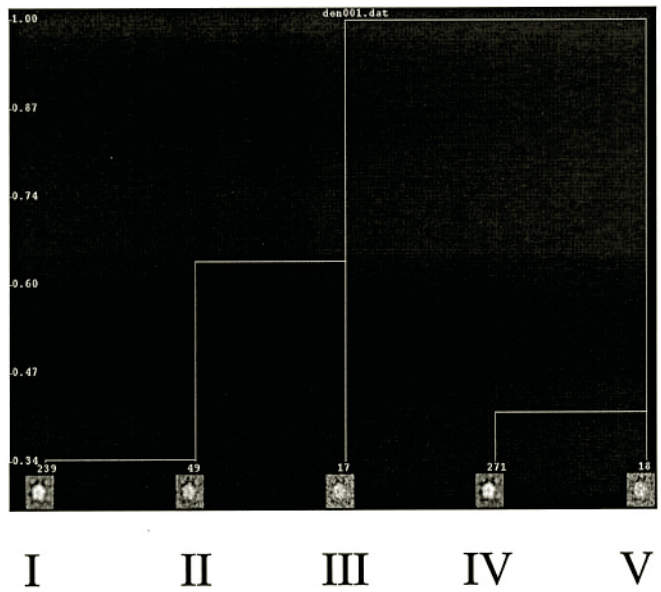

FIG. 3. **Definition of particle classes after single-particle analysis.** A linkage tree was obtained from hierarchical ascendant classification using complete linkage as a merging criterion. The cutting level was 0.34, which generated a suitable within-group resolution of the major classes (see "Results"). The number of particles within each class is indicated *above* the images.

orientated differently with respect to the incident electron beam, but the high degree of homogeneity of the protein was shown by the consistent size of the protein molecules, with most molecules having a maximal diameter of ~100 Å. Rotational and translational alignment followed by multivariate statistical analysis of the images of selected particles enabled differences in the images to be analyzed. This allowed the particles to be classified according to the orientation of the particle (*e.g. top* and *side views*), which were separated by correspondence analysis followed by hierarchical ascendant classification (29, 31). Images that were similar were merged together to form similar projections or classes (35, 36) and after further rounds of rotational and translational alignment were finally averaged. The class averages thus showed the most commonly occurring projections with a concomitant improvement in the signal-to-noise ratio. This algorithm was implemented using SPIDER (31, 34) using a reference-free-based alignment method (35, 36), which offers the advantage of the final image not being dominated by a chosen reference. The assignment into various classes of projection at a cutoff level of 0.34 is represented by the *dendrogram* shown in Fig. 3. Various projections are shown by classes I–V. Each of the two major classes (I and IV) had a good within-group resolution (22 Å) as judged by Fourier Ring Correlation (31, 34). There appears to be mainly face-on views of MRP1 with side-on views (where the molecule would be likely to display a rectangular appearance perpendicular to the incident electron beam) appearing less frequently probably due to preferred orientations of MRP1 on the grid surface. The three projection maps corresponding to the three most populous classes (I, II, and IV) are shown in Fig. 4*a*, *b*, and *c*, respectively.

Fig. 4 (*a* and *c*) shows that the predominant projection of MRP1 was toroidal in shape similar to that observed earlier for P-gp (29) with a ring of protein comprised of five or six densities surrounding a central stain filled region of ~35-Å diameter. The handedness of these class averages was thought to be an "up" view (see below). Some protein densities appear to be roughly related by pseudo-2-fold symmetry, although the overall shape of this average is approximately pentagonal. A rotational autocorrelation match and rotational filtering, implemented by RFILTIMPER in MRC (see below), suggested there was some 2- and 5-fold symmetry in MRP1 (data not shown). The averaged projection structure shows a relatively open arrangement of protein densities surrounding the outer perimeter. Fig. 4*b* shows a view, which appears distinctive from Fig. 4 (*a* and *c*) and is calculated from relatively fewer particles, and hence the resolution was ~35 Å. The *asterisks* show two densities related by 2-fold pseudosymmetry. The third NH_2-terminal MSD of MRP1 might be expected to reduce any pseudo-2-fold symmetry (40). An indication from these projection maps for such behavior is in Fig. 4*b* where the density labeled *3* sits somewhat apart from the densities *1*, *2*, *4*, and *5*. Density *3* in Fig. 4*a* also remains apart from its neighboring densities, whereas density *4* protrudes more from the perimeter of the protein ring.

Two-dimensional Crystals of MRP1—Because of the high degree of homogeneity of the purified MRP1, attempts were made to grow two-dimensional crystals of the protein by Bio-beads-assisted detergent removal at a suitable ratio of protein to lipid. This allowed us to establish whether a higher resolution structure of MRP1 would be attainable by electron cryomicroscopy. Fig. 5 shows a small two-dimensional crystal of MRP1 with lattice dimensions 133 × 256 Å. Low dose images of vesicles from several crystallization trials showed two-dimensional arrays displaying order to ~25 Å as judged by optical diffraction. After correction for lattice distortions using image processing, structure factors were found to ~20-Å resolution. A typical plot of a computed Fourier transform for one of the

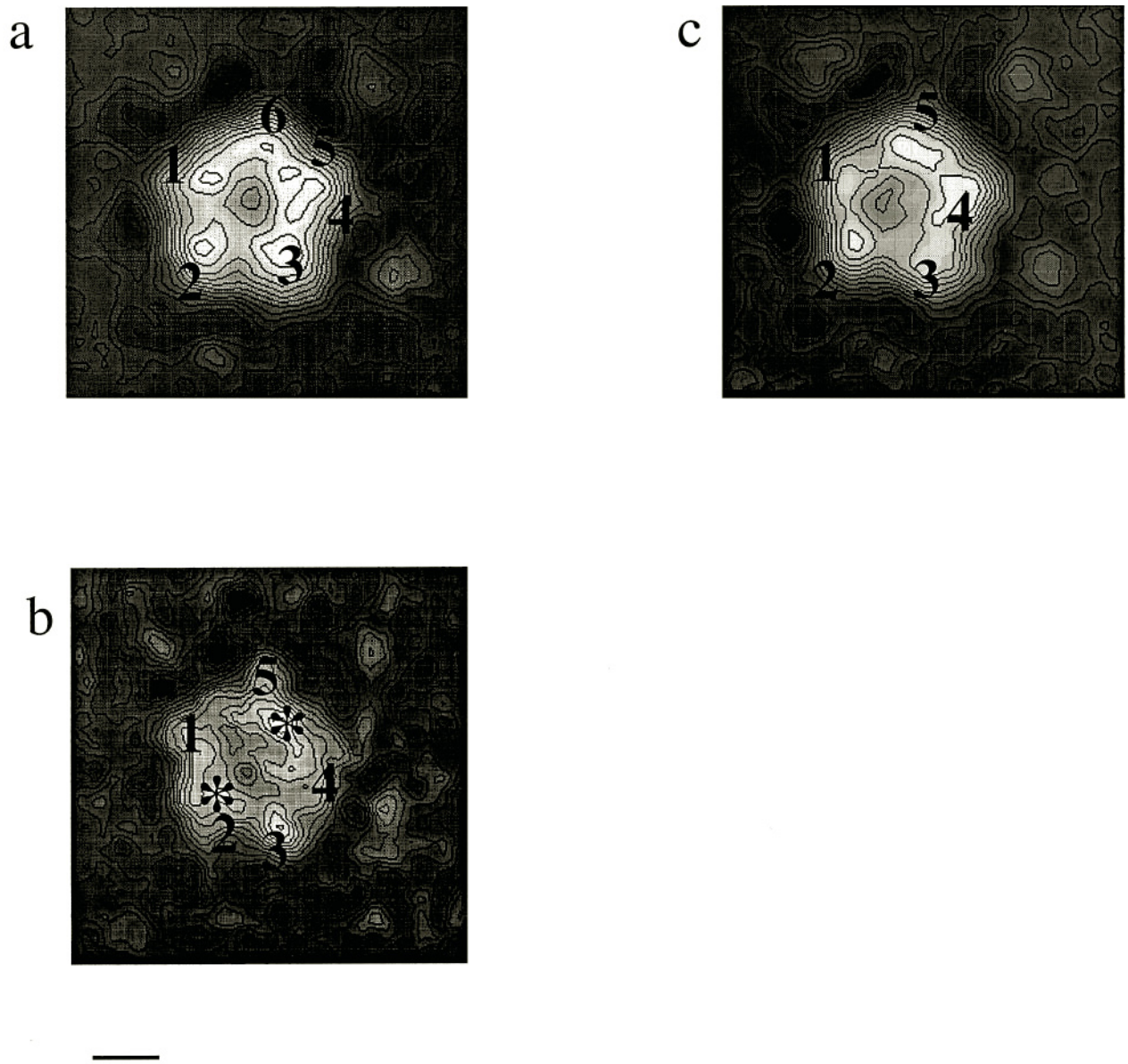

FIG. 4. **Projection maps of solubilized MRP1 calculated by single-particle analysis.** Images of 600 particles were classified into subgroups using SPIDER. The stain is delineated in *black* and the protein in *white*. The three major classes of MRP1 particles (*a–c*), which differ in their orientation with respect to the electron beam, are shown. The *scale bar* represents 39 Å.

crystals is depicted in Fig. 6 with high signal-to-noise (IQ 3) (41, 42) reflections detected up to a resolution of ~20 Å. Initial analysis on the basis of phase comparisons suggested *p*2 symmetry could be present (37). Projection maps of MRP1 crystals, with data truncated at ~25-Å resolution with no symmetry (*p*1) (Fig. 7*a*) and with *p*2 symmetry enforced (Fig. 7*b*) are shown after merging data from three independent lattices. In Fig. 7*b* the putative monomer is outlined. The unit cell appears to contain two MRP1 molecules, related by a crystallographic 2-fold axis perpendicular to the membrane. The molecular boundaries of a monomer (outlined) were apparent. The projection map suggests that the intermonomer contacts are more extensive on one side of MRP1. The projection map appears distinct from those calculated by single-particle analysis, and it is possible to explain these differences in accordance with stain distribution at the intracellular as opposed to the extracellular surface for the single-particle map (see "Discussion"). The quality of the merged projection map can be judged from the statistics shown in Table I. The overall *p*2 phase residual to 20-Å resolution was 21° (where 45° is random or non *p*2 phases) providing confidence in the structure obtained and the plane group assignment.

DISCUSSION

Since the cloning of MRP1 from the human small cell lung cancer cell line H69AR, expression of this ABC transporter has been widely detected in both resistant tumor cell lines and clinical samples (1, 6, 12) similar to that observed for P-gp (10). Here, we report the first projection structure of MRP1 to ~22-Å resolution determined by single-particle analysis and electron crystallography. The MRP1 used in this study was purified from H69AR lung cancer cells and retains its ATPase and transport activities as well as its reactivity with antibodies that recognize conformation-dependent epitopes, demonstrating that it remains folded in an active configuration (24, 28, 39).

In the present study MRP1 appears to be monomeric after detergent solubilization and isolation but dimeric upon reconstitution into crystalline protein/lipid arrays (Fig. 7), which may have important functional implications. Whether MRP1 is dimeric in native membranes is not known at present, because

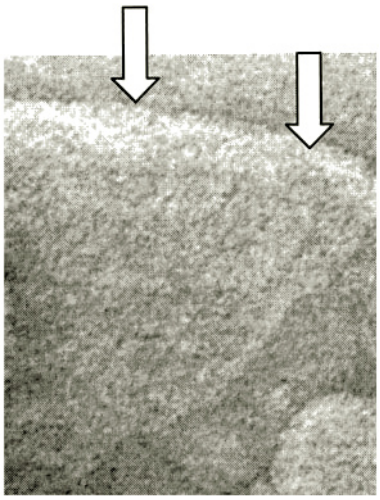

FIG. 5. **Electron micrograph of two-dimensional crystals of dimyristoyl L-α-phosphatidylcholine vesicles containing MRP1 (1:1, protein:lipid, w/w) stained with 2% w/v uranyl acetate.** The *white arrows* indicate the two-dimensional crystal. The *scale bar* corresponds to 500 Å.

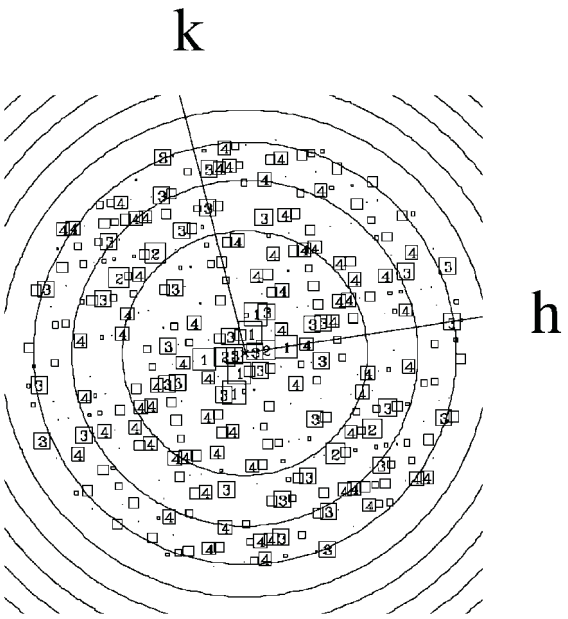

FIG. 6. **A computer-generated Fourier transform of an image of a single two-dimensional crystal.** The data shown was obtained after three cycles of lattice unbending, which compensates for distortion in the crystal lattice by applying the lattice vectors of an ideal lattice usually selected from the center of the crystal to the remainder of the crystalline area. The *numbers* in the *boxes* indicate the quality of the reflection with *large squares* and *low numbers* indicating reflections of high signal-to-noise ratio (IQ) (41, 42). The IQ value represents the signal-to-noise above background with a lower IQ value (*e.g. 1–4*) representing a good signal-to-noise ratio of the reflection whereas a higher IQ value (*e.g. 7–8*) represents a poor one. The *arrows* indicate the direction of the reciprocal lattice vectors (*h* and *k*), and the *circles* represent zero values in the contrast transfer function. The edge of the plot corresponds to a resolution of ~20 Å.

the dimer observed in these projection maps may simply reflect favorable crystallographic interactions. However, earlier radiation inactivation studies have suggested MRP1 can function as a dimer in the membrane (43). The cystic fibrosis transmembrane regulator (CFTR), which belongs to the same subfamily C of the ABC transporters as MRP1, also appears to possess a dimeric character when bound to a recombinant CAP70 protein (44). A dimeric association for CFTR has been further implied from experiments using a fusion protein consisting of two tandemly linked CFTR coding sequences (45) and by electron microscopy studies (46). However, other biochemical studies using monoclonal antibodies have proposed a monomeric form for CFTR (47). Structural studies for P-gp, which is structurally more dissimilar to MRP1 than CFTR, have shown that it exists as a monomer as both single particles and in two-dimensional crystals, although the crystals contained no lipid (29).[2]

The single-particle images could readily pack into the crystal lattice shown in Fig. 7, and the size of the MRP1 monomer from the two-dimensional crystals closely matched the longest dimension (100 Å) for the single particles along *b*, whereas the dimensions along *a* were slightly smaller (70 Å). Negative stain, however, is unlikely to penetrate the sealed liposomes and, consequently, projection maps will tend to be dominated by the protein domains exposed on the outer surface of the liposomes. Thus, if the protein domains are only partially exposed along *a*, then this may account for the difference along this direction. For the detergent-solubilized MRP1, a toroidal ring of protein surrounds a large (35 Å in diameter) stain-filled region, which is not detected for the crystals. This could be explained, if the view for the single particles represents predominantly the extracellular surface of the molecule and the two-dimensional crystals shows the intracellular surface exposed outside the liposomes, which is dominating the projection. Reconstitution experiments by Manciu *et al.* (48) using similar conditions to those described here showed that MRP1 inserted into liposomes in an inside-out configuration, with its catalytic sites or NBDs outside the liposomes. These findings suggest that the projection maps derived from the two-dimensional crystals could be representative of the stain distribution at the intracellular surface of MRP1 (Fig. 7). The monomer appears to contain 2 pseudosymmetrical domains that could be consistent with this interpretation. Similar features are observed for the intracellular surface of P-gp crystals, which showed two pseudosymmetrical densities separated by ~90 Å. These were assigned as the NBDs because the x-ray crystal structure of the NBDs of histidine permease (49) could be comfortably docked with them.[2] In contrast, the extracellular surface of P-gp is characterized by a toroidal ring of protein densities with a large central depression, similar to that observed for MRP1. Because the extracellular surface of MRP1 could associate preferentially with the specimen support film, possibly because of its surface charges, this region could be the most strongly stained, and thus it is feasible that features on this side of the molecule could dominate a projection from single particles. Our preliminary interpretation is that MRP1 is structurally similar to P-gp (29),[2] with a large extracellular pore surrounded by a ring of protein, with the pore sealed on the intracellular side by its two NBDs. This working model will be tested in the future by electron cryomicroscopy of unstained specimens and by three-dimensional reconstructions.

Several MRP-related ABC proteins that have been characterized are organic anion transporters, and thus their relatively hydrophilic substrates do not readily penetrate the cell membrane. The large putative pore in MRP1 might facilitate transport of these charged substrates. The putative pore opens at the extracellular face of the membrane, but it vastly exceeds the diameter required for the passage of known MRP1 substrates and opening of such a pore across the membrane would obviously not be compatible with cell viability. However, our studies from P-gp and now from MRP1 two-dimensional crystals suggest that the pore of this protein is closed at the cytoplasmic face of the membrane by either the intracellular hy-

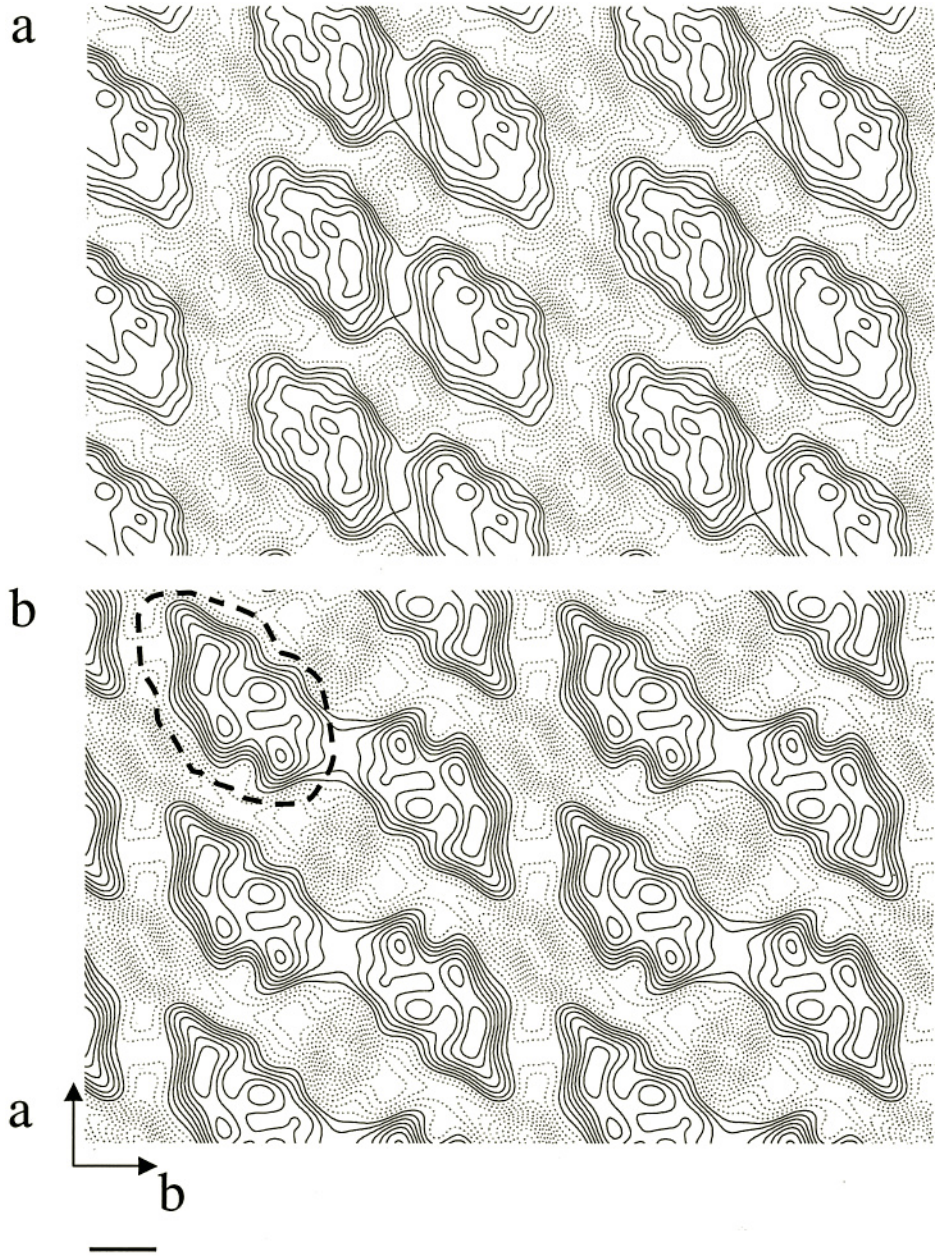

FIG. 7. **Projection maps of MRP1 in negative stain at 25-Å resolution calculated from images of two-dimensional crystals of MRP1.** In *a* no symmetry (*p*1) and in *b* *p*2 symmetry is enforced. Data from a single crystal (*a*) and data from amplitudes and phases merged from three independent lattices (*b*) are shown. One unit cell contains two molecules of MRP1. The *solid lines* indicate density above the mean with contours extending up to 1.5 sigma in six even steps; *dotted lines* indicate density below the mean value. A putative monomer is shown by the *dotted lines*. In *a*, 2-fold axes of symmetry are evident. In *b*, the phases were constrained to 0° or 180°, and the projection is centrosymmetric. The *scale bar* corresponds to 30 Å.

TABLE I
Crystallographic data for negatively stained images of MRP1

Unit cell parameters	a = 139 ± 2Å b = 256 ± 2Å γ = 86.0° ± 3°
Number of images	3
Number of unique reflections (to IQ 7)	87
Phase error to 20 Å after rounding to 0/180° (IQ 7 max, 45° is random)	21°

drophilic loops and/or the NBDs (29).[2] The NBDs of MRP1 could serve a similar function, although it should be borne in mind that the two NBDs of MRP1 are considerably more divergent than those of P-gp and appear to be more functionally distinct with respect to their ATP binding and hydrolysis properties (50–52).

The various projection maps appear to suggest that MRP1 exhibits some 2-fold pseudosymmetry, which may be explained by the core structure comprising two MSDs each consisting of

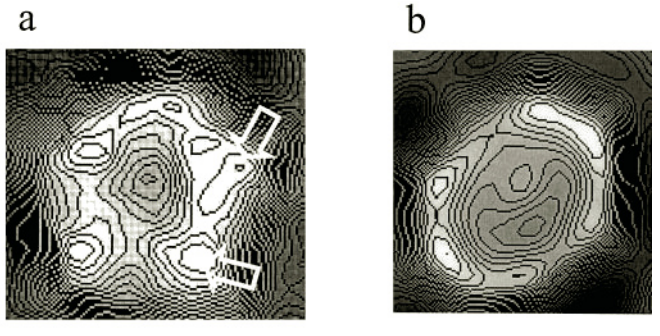

FIG. 8. **Comparison of solubilized MRP1 (*a*) and P-gp (*b*) projection structures predicted to correspond to the extracellular face of the proteins (see "Discussion").** Both structures were filtered to the same resolution and similarly contoured to facilitate a comparison between the two. The projection in *a* corresponds to the class shown in Fig. 4*a*. P-gp data are from previous studies (29, 30). The *scale bar* corresponds to 22 Å.

six transmembrane segments and two NBDs. This was supported by the rotational autocorrelation search and rotational filtering for the single-particle-derived data and the two-dimensional crystals, respectively, described earlier. The NH_2-terminal MSD1 comprised of five transmembrane segments found in MRP1 might be expected to cause the protein to deviate from 2-fold pseudosymmetry, and this is supported by the observation of some 5-fold pseudosymmetry in the autocorrelation search for the single-particle data. The protrusion on density *4* and the additional density *3* (Fig. 4) also supports a deviation from 2-fold pseudosymmetry. Fig. 8 shows a comparison of solubilized P-gp and MRP1 structures in projection, truncated at approximately the same resolution (22 Å) where the major differences are highlighted (see *arrows*). It is possible to speculate that density *3* and/or *4* (Fig. 4) might correspond to the MSD1 of MRP1 and this requires further investigation. For example, previous studies have shown that MRP1, which has been NH_2-terminally truncated at amino acid position 204, and thus lacking MSD1, retains its ability to transport LTC_4 (21). It could be of future interest to determine the structure of this truncated MRP1 to establish how it compares with that of the full-length protein.

In conclusion, this work represents the first structure of a protein from the MRP subfamily C of the ABC transporter superfamily that differs in its general architecture from that of P-gp. Dimeric characteristics of MRP1 appear after reconstitution into lipid bilayers, although its *in vivo* oligomeric form is still not known. Our data are in agreement with most of the biochemical evidence available for MRP1. This structural data should contribute to a greater understanding of the substrate binding and transport mechanism of MRP1 and related ABC transporters.

Acknowledgments—We are grateful to the Royal Society (London) for a travel grant (to M.F.R.) and to Dr. A. Kitmitto and Giles Velarde (University of Manchester Institute of Science and Technology) for useful discussions.

REFERENCES

1. Cole, S. P. C., Bhardwaj, G., Gerlach, J. H., Mackie, J. E., Grant, C. E., Almquist, K. C., Stewart, A. J., Kurz, E. U., Duncan, A. M. V., and Deeley, R. G. (1992) *Science* **258,** 1650–1654
2. Nooter, K., Westerman, A. M., Flen, M. J., Zaman, G. J. R., Scheper, R. J., van Wingerden, K. E., Burger, H., Oostrum, R., Boersma, T., Sonneveld, P., Gratama, J. W., Kok, T., Eggermont, A. M. M., Bosman, F. T., and Stoter, G. (1995) *Clin. Cancer Res.* **1,** 1301–1310
3. Norris, M. D., Bordow, S. B., Marshall, G. M., Haber, P. S., Cohn, S. L., and Haber, M. (1996) *N. Engl. J. Med.* **334,** 231–238
4. Chan, H. S. L., Lu, Y., Grogan, T. M., Haddad, G., Hipfner, D. R., Cole, S. P. C., Deeley, R. G., Ling, V., and Gallie, B. L. (1997) *Cancer Res.* **57,** 2325–2330
5. Kreisholt, J., Sorensen, M., Jensen, P. B., Nielsen, B. S., Andersen, C. B., and Sehested, M. (1998) *Br. J. Cancer* **77,** 1469–1473
6. Hipfner, D. R., Deeley, R. G., and Cole, S. P. C. (1999) *Biochim. Biophys. Acta* **1461,** 359–376
7. Cole, S. P. C., Sparks, K. E., Fraser, K., Loe, D. W., Grant, C. E., Wilson, G. M., and Deeley, R. G. (1994) *Cancer Res.* **54,** 5902–5910
8. Zaman, G. J. R., Flens, M. J., van Lensden, M. R., de Haas, M., Mulder, H. S., Lankelma, J., Pinedo, H. M., Scheper, R. J., Baas, F., Broxterman, H. J., and Borst, P. (1994) *Proc. Natl. Acad. Sci. U. S. A.* **91,** 8822–8826
9. Sharom, F. J. (1997) *J. Membr. Biol.* **160,** 161–175
10. Ambudkar, S. V., Dey, S., Hrycyma, C. A., Ramachandra, M., Pastan, I., and Gottesman, M. M. (1999) *Annu. Rev. Pharmacol. Toxicol.* **39,** 361–398
11. Holland, I. B., and Blight, M. A. (1999) *J. Mol. Biol.* **293,** 381–399
12. Borst, P., Evers, R., Kool, M., and Wijnholds, J. (1999) *Biochim. Biophys. Acta* **1461,** 347–357
13. Zielenski, J., and Tsui, L.-C. (1995) *Annu. Rev. Genet.* **29,** 777–807
14. Bryan, J., and Aguilar-Bryan, L. (1997) *Curr. Opin. Cell Biol.* **9,** 553–559
15. Stride, B. D., Valdimarsson, G., Gerlach, J. H., Wilson, G. M., Cole, S. P. C., and Deeley, R. G. (1996) *Mol. Pharmacol.* **49,** 962–971
16. Bakos, E., Hegedus, T., Hollo, Z., Welker, E., Tusnady, G. E., Zaman, G. J. R., Flens, M. J., Varadi, A., and Sarkadi, B. (1996) *J. Biol. Chem.* **271,** 12322–12326
17. Hipfner, D. R., Almquist, K. C., Leslie, E. M., Gerlach, J. H., Grant, C. E., Deeley, R. G., and Cole, S. P. C. (1997) *J. Biol. Chem.* **272,** 23623–23630
18. Kast, C., and Gros, P. (1998) *Biochemistry* **37,** 2305–2313
19. Hipfner, D. R., Almquist, K. C., Stride, B. D., Deeley, R. G., and Cole, S. P. C. (1996) *Cancer Res.* **56,** 3307–3314
20. Gao, M., Yamazaki, M., Loe, D. W., Westlake, C. J., Grant, C. E., Cole, S. P. C., and Deeley, R. G. (1998) *J. Biol. Chem.* **273,** 10733–10740
21. Bakos, E., Evers, R., Szakacs, G., Tusnady, G. E., Welker, E., Szabo, K., de Haas, M., van Deemer, L., Borst, P., Varadi, A., and Sarkadi, B. (1998) *J. Biol. Chem.* **273,** 32167–32175
22. Leier, I., Jedlitschky, G., Buchholz, U., Cole, S. P. C., Deeley, R. G., and Keppler, D. (1994) *J. Biol. Chem.* **269,** 27807–27810
23. Leier, I., Jedlitschky, G., Buchholz, U., Center, M., Cole, S. P. C., Deeley, R. G., and Keppler, D. (1996) *Biochem. J.* **314,** 433–437
24. Mao, Q., Deeley, R. G., and Cole, S. P. C. (2000) *J. Biol. Chem.* **275,** 34166–34172
25. Loe, D. W., Almquist, K. C., Deeley, R. G., and Cole, S. P. C. (1996) *J. Biol. Chem.* **271,** 9675–9682
26. Loe, D. W., Deeley, R. G., and Cole, S. P. C. (1998) *Cancer Res.* **58,** 5130–5136
27. Renes, J., de Vries, E. G. E., Nienhuis, E. F., Jansen, P. L. M., and Muller, M. (1999) *Br. J. Pharmacol.* **126,** 681–688
28. Mao, Q., Leslie, E. M., Deeley, R. G., and Cole, S. P. C. (1999) *Biochim. Biophys. Acta* **1461,** 69–82
29. Rosenberg, M. F., Callaghan, R., Ford, R. C., and Higgins, C. F. (1997) *J. Biol. Chem.* **272,** 10685–10694
30. Higgins, C. F., Callaghan, R., Linton, K. J., Rosenberg, M. F., and Ford, R. C. (1997) *Semin. Cancer Biol.* **8,** 135–142
31. Frank, J. (1996) *Three-dimensional Electron, Microscopy of Macromolecular Assemblies*, Academic Press, San Diego
32. Walz, T., and Grigorieff, N. (1998) *J. Struct. Biol.* **121,** 142–161
33. Crowther, R. A., Henderson, R., and Smith, J. M. (1996) *J. Struct. Biol.* **116,** 9–16
34. Frank, J., Radermacher, M., Penczek, P., Zhu, J., Li, Y. H., Ladjadj, M., and Leith, A. (1996) *J. Struct. Biol.* **116,** 190–199
35. Penczek, P., Radermacher, M., and Frank, J. (1992) *Ultramicroscopy* **40,** 33–53
36. Penczek, P. A., Grassucci, R. A., and Frank, J. (1994) *Ultramicroscopy* **53,** 251–270
37. Valpuesta, J. M., Carrascosa, J. L., and Henderson, R. (1994) *J. Mol. Biol.* **240,** 281–287
38. Bailey, S. (1994) *Acta Crystallogr. Sect. D Biol. Crystallogr.* **50,** 760–763
39. Hipfner, D. R., Mao, Q., Qiu, W., Leslie, E. M., Gao, M., Deeley, R. G., and Cole, S. P. C. (1999) *J. Biol. Chem.* **274,** 15420–15426
40. Rosenberg, M. F., Holzenburg, A., Shepherd, F. H., Nicholson, W. V., Flint, T. D., and Ford, R. C. (1997) *Biochim. Biophys. Acta* **1319,** 119–132
41. Henderson, R., Baldwin, J. M., Downing, K. H., Lepault, J., and Zemlin, F. (1986) *Ultramicroscopy* **19,** 147–178
42. Henderson, R., Baldwin, J. M., Ceska, T. A., Zemlin, F., Beckmann, E., and Downing, K. H. (1990) *J. Mol. Biol.* **213,** 899–929
43. Soszynski, M., Kaluzna, A., Rychlik, B., Sokal, A., and Bartosz, G. (1998) *Arch. Biochem. Biophys.* **354,** 311–316
44. Wang, S. S., Yue, H. W., Derin, R. B., Guggino, W. B., and Lit, M. (2000) *Cell* **103,** 169–179
45. Zerhusen, B., Zhao, J. Y., Xie, J. X., Davis, P. B., and Ma, J. J. (1999) *J. Biol. Chem.* **274,** 7627–7630
46. Eskandari, S., Wright, E. M., Kreman, M., Starace, D. M., and Zampighi, G. A. (1998) *Proc. Natl. Acad. Sci. U. S. A.* **95,** 11235–11240
47. Marshall, J., Fang, S., Ostedgaard, L. S., Oriordan, C. R., Ferrara, D., Amara, J. F., Hoppe, H., Scheule, R. K., Welsh, M. J., Smith, A. E., and Cheng, S. H. (1994) *J. Biol. Chem.* **269,** 2987–2995
48. Manciu, L., Chang, X. B., Riordan, J. R., and Ruysschaert, J. M. (2000) *Biochemistry* **39,** 13026–13033
49. Hung, L. W., Wang, I. X. Y., Nikaido, K., Liu, P. Q., Ames, G. F. L., and Kim, S. H. (1998) *Nature* **396,** 703–707
50. Gao, M., Cui, H. R., Loe, D. W., Grant, C. E., Almquist, K. C., Cole, S. P. C., and Deeley, R. G. (2000) *J. Biol. Chem.* **275,** 13098–13108
51. Nagata, K., Nishitani, M., Matsuo, M., Kioka, N., Amachi, T., and Ueda, K. (2000) *J. Biol. Chem.* **275,** 17626–17630
52. Hou, Y. X., Cui, L., Riordan, J. R., and Chang, X. B. (2000) *J. Biol. Chem.* **275,** 20280–20287